

Mathematical Determination of a Flute, Construction of a CAD Model, and Determination of the Optimal Geometric Features of a Microdrill

Teshome Mulatie Bogale¹ · Fang-Jung Shiou¹ · Geo-Ry Tang¹

Received: 7 September 2014 / Accepted: 12 March 2015 / Published online: 26 March 2015
© King Fahd University of Petroleum & Minerals 2015

Abstract The objective of this paper was to determine mathematically a flute, to construct a CAD model and to determine the optimal geometric features of a 0.1 mm diameter of a microdrill based on the stress analysis. The flute of a microdrill was determined mathematically by defining the undercutting relative positions of both the microdrill and grinding wheel and their profiles with respect to setting angle. The mathematically determined flute was used to construct a CAD model of a microdrill using Pro/Engineer software. The cross-sectional comparison between the model and fabricated microdrill was carried out by cutting at different lengths, and the results of the web thickness of the model and the fabricated microdrill were approximately the same. Similarly, the images of primary flank areas and secondary flank areas of fabricated microdrills were taken using optical microscope, and they were compared with the shapes of cutting edge, chisel edge, primary flank areas and secondary flank areas of the model. Based on this comparison, they were almost the same. Hence, the consideration of the mathematically determined flute for the construction of the CAD model of a microdrill was feasible. The optimal geometric features of a microdrill have been determined by setting design control parameters for geometric features and carrying out optimization of the stress/displacement analysis using Pro/Mechanica software so that the maximum Von Mises stress of the microdrill was minimized below the compressive strength of the material property.

Keywords Flute · CAD model · Optimal geometrical features · Microdrill · Pro/Mechanica software

1 Introduction

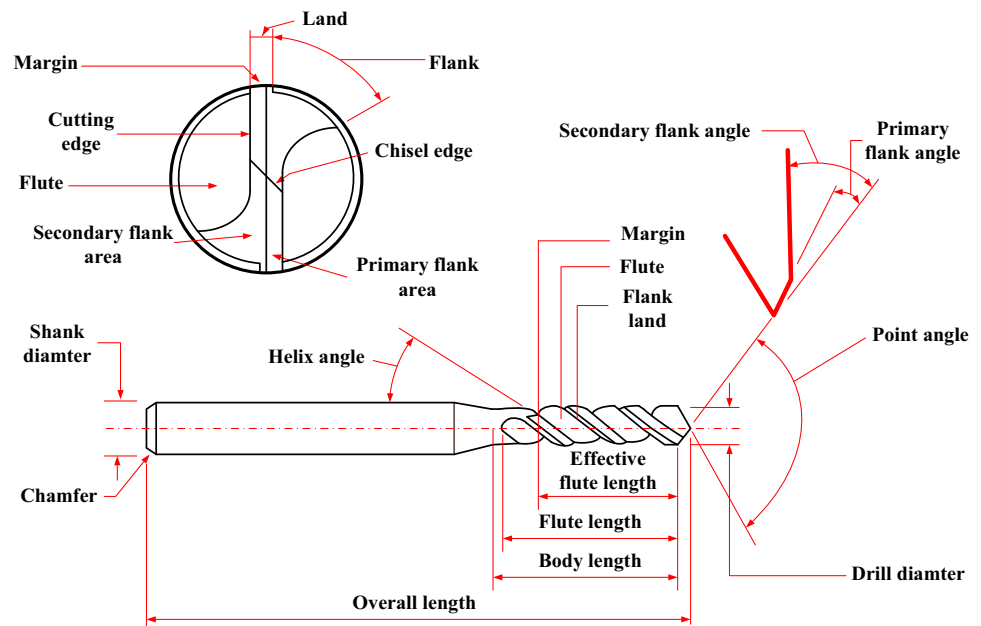
Microdrilling plays significant roles in the industrial application, such as the micro-holes on a nozzle tip of fuel injector, a hydraulic valve and a printed circuit board (PCB), in recent years. Microdrilling or through-hole drilling of PCBs has advantages to produce an opening through the board that will permit a subsequent process to form an electrical connection between top, bottom and internal conductor pathways, and to permit through the board component mounting with structural integrity and precision of location as Coombs [1] had stated in 2007. Zheng et al. [2] stated that with trends toward “lighter, thinner and smaller” electronic products, PCBs require smaller holes to be drilled in a more limited area. Among the available industrial microdrilling processes, such as micro-EDM, mechanical drilling, laser beam drilling and electron beam drilling, high-speed mechanical drilling is the most economical and commonly used for drilling micro-holes using microdrills.

The geometric attributes of a microdrill was explained by Coombs [1] in 2007, and nomenclature of the microdrill is shown in Fig. 1. Although many researchers [3,4] studied about the coating of drills to increase strength, Coombs investigated the best material for microdrills that are used to drill PCBs. According to his study, the recommended material of a microdrill is tungsten carbide because of its wear resistance and low cost. The compromise of this very hard (carbide) material is that it is also brittle and subject to damage in the form of chips if not handled carefully. The mathematical model of a microdrill is directly dependent on the grinding wheel of the microdrill. Several researchers in previous studies [5–9]

✉ Fang-Jung Shiou
shiou@mail.ntust.edu.tw

¹ Department of Mechanical Engineering, National Taiwan University of Science and Technology, # 43, Section 4, Keelung Rd. Da’an Dist., Taipei City 106, Taiwan, ROC

Fig. 1 Microdrill geometry



presented a mathematical model on the point geometry of a drill and explained that the performance of drill is influenced due to different drill point geometries and grinding process. The influence of the shapes of chisel edge and cutting lips on the improvement of a twist drill point geometry was also investigated in 2005 by Paul et al. [10]. The twist drill point geometry was analyzed by several researchers in [11, 12] with respect to the drill flute and flank contours by considering cross sections of the drill cut by planes perpendicular to its axis. Several researchers [13, 14] studied a CAD approach for a generalized helical groove-machining model based on the establishment of the fundamental conditions of engagement between the generating tool surfaces and generated helical groove surface. Kang et al. [15] investigated a mathematical analysis that was presented as the basis for a CAD/CAM system for design and manufacture of components with helical grooves in 1997. Kaldor et al. [16] introduced two methods in 1988, the “direct” and the “indirect” that allow for the prediction of the helical flute profiles and cutter profiles, respectively. However, there is not any study conducted specifically on the mathematical determination of the flute of the microdrill.

A mathematical model of the grinding wheel profile required for a specific twist drill flute was described in 1982 by Radhakrishnan et al. [17]. The definition of the grinding wheel for the manufacture of drill flute based on differential geometry and kinematics was studied in 1990 by Ehmann and DeVries [18], and theoretical contour of grinding wheel profile was explained in 2011 by Chang et al. [19]. Although there are investigations on grinding wheel as we mentioned some of them above, there is not any specific study conducted by defining the undercutting relative positions of both the mi-

crodrill and grinding wheel and their profiles with respect to setting angle to figure out the shape of flute clearly.

Optimization of a microdrill is the ultimate method to increase the tool life and maintain the through-hole quality of a PCB. Hence, loads on the microdrill during drilling must be calculated with respect to cutting/drilling pressure, feed, length of chisel edge, diameter of microdrill and point angle to minimize the amount of stress on the microdrill. Some of the studies on optimization of drill are stated below. Hinds and Treanor [20] explained the analysis of stress using finite element method on a microdrill to reduce the possibility of drill breakage in 2000, and also, Chen [21] applied finite element method to drill design based on deformation in 1997. Several researchers [22–25] wrote the optimization and simulation of geometry of drill. Shiou and Hung [26] introduced the determination of the optimal geometrical features of a microdrill based on stress/displacement analysis. Nowadays, there is not any investigation on calculation of the loads (thrust and torque) on the microdrill and comprehensive configurations of the design control parameters for determination of the optimal geometric features during optimization of a microdrill.

The objectives of this study are to determine the flute mathematically by defining the undercutting relative positions of both the microdrill and grinding wheel and their profiles with respect to setting angle, and to construct a CAD model based on a mathematically determined flute of a 0.1 mm diameter of microdrill. After construction of CAD model, comparison of the cross section and shapes of the CAD model with a fabricated 0.1 mm diameter of microdrill is carried out. This study also points out the optimal geometric features under stress/displacement analysis using Pro/Mechanica software

by calculating the values of loads on microdrills and configuring the design control parameters of the geometric features.

This paper describes about the materials and methods of modeling of the microdrill, constraints and loads on the microdrill, initial static analysis, configuration of the design control parameters, sensitivity study analysis of the configured design control parameters and optimization analysis of the geometric features of the microdrill first. Next, the results and discussion of the mathematical determination of a flute, construction of a CAD model and determination of the optimal geometric features of a microdrill are presented in detail. Finally, conclusion is presented.

2 Modeling of the Microdrill

2.1 Mathematical Determination of the Flute of the Microdrill

According to Fig. 2 which shows the illustration of undercutting of a microdrill with grinding wheel, the center of microdrill is point O of XYZ coordinate system, the center of wheel is point O' , and point O'' is the center of wheel profile. Dimensions of both microdrill and grinding wheel parameters to determine flute of a microdrill mathematically are listed in Table 1. Consider any arbitrary point on microdrill cross section along Z axis $(0, 0, u)$ as shown in Fig. 3a;

$$t \leq u \leq R_d, \tag{1}$$

According to Fig. 3a, point $M(M_X, M_Y, M_Z)$ is on the elliptical arc on the microdrill cross section with helix angle,

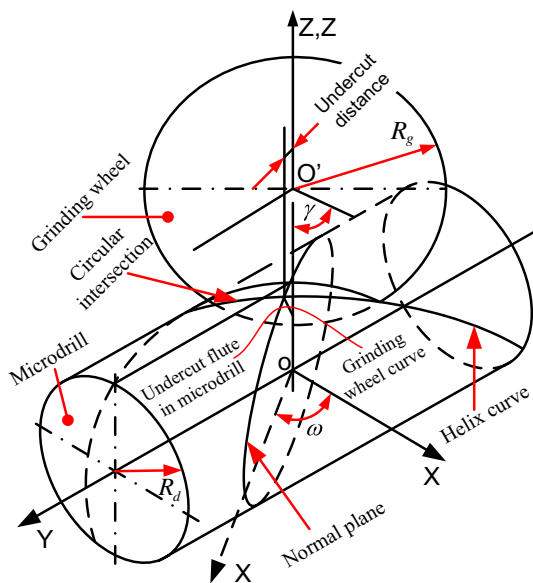


Fig. 2 Illustration for microdrill undercutting with a grinding wheel

Table 1 Parameters and their dimensions

Part	Dimension	Parameter	Value
Microdrill	Drill diameter ($d = 0.1$ mm)	$R_d = d/2$	0.05 mm
	Web thickness ($w = 0.05$ mm)	$t = w/2$	0.025 mm
	Helix angle ($\theta = 45^\circ$)	$\omega = \theta$	0.785398 rad
Grinding wheel	Diameter ($D_g = 150$ mm)	$R_g = D_g/2$	75 mm
	Thickness	t_g	1 mm
	Small (right) radius of the contour,	R_1	0.0185 mm
	Large (left) radius of the contour	R_2	0.0790 mm
	Small radius central angle ($\alpha_1 = 65^\circ$)	α_1	1.134464 rad
	Large radius central angle ($\alpha_2 = 48^\circ$)	α_2	0.837758 rad
Setting angle ($\gamma = 52^\circ$)	γ	0.907571 rad	

and the angle between OM and Y axis is θ . The position of point M with respect to axes is expressed as

$$M_X = 0, \tag{2}$$

$$M_Y = -(u/\sin \omega) \cos \theta, \tag{3}$$

$$M_Z = u \sin \theta, \tag{4}$$

Based on the Eq. (1), it is possible to find the minimum and maximum value of θ by taking any point on the circular arc of the microdrill cross section. The empirical formulas are as follows:

$$\theta_{\min} = \arcsin(t/u), \tag{5}$$

$$\theta_{\max} = \pi - \arcsin(t/u), \tag{6}$$

The optimal value of θ was solved iteratively. Based on the definition of the grinding wheel as shown in Fig. 3b, point P on the grinding wheel is the same as the point M on microdrill on the YZ plane. Therefore, the components of point $P(P_X, P_Y, P_Z)$ are described using Eqs. (2)–(4) on the left radius R_2 of the grinding wheel as follows:

$$P_X = 0, \tag{7}$$

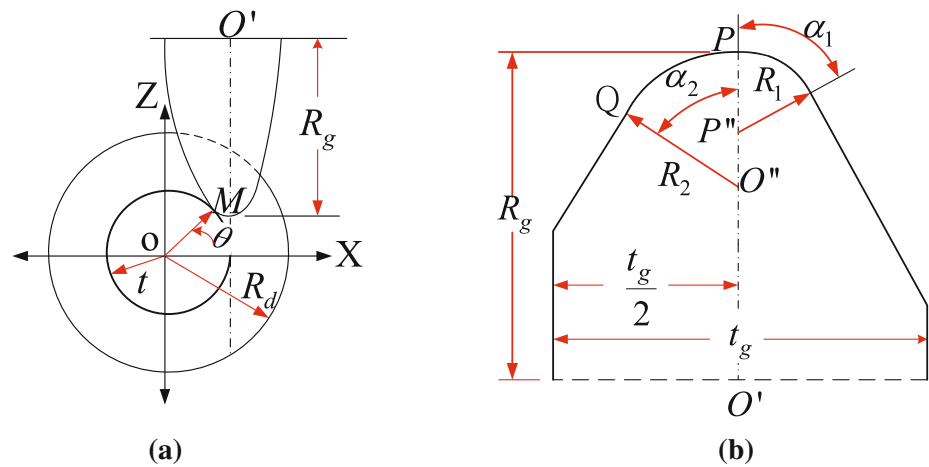
$$P_Y = M_Y, \tag{8}$$

$$P_Z = M_Z, \tag{9}$$

Let us designate β as an angle between $O'P$ and Z axis, and β and $O'P$ become as

$$\beta = \arctan \left(\frac{P_Y}{R_g + R_2 - P_Z} \right), \tag{10}$$

Fig. 3 Definitions: **a** microdrill, and **b** grinding wheel



$$P_r = O'P = \sqrt{\left((R_g + t - P_z)^2 + P_y^2\right)}, \quad (11)$$

The angle between $O''Q$ and $O'P'$ (where point P' on the surface of the unsettled wheel point P'' is the projection of P' on YZ plane) α is expressed using the following equation:

$$\alpha = \arccos\left(1 - \frac{(R_g - P_r)}{R_2}\right), \quad (12)$$

The contact point $Q(Q_X, Q_Y, Q_Z)$ on the on the left arc, radius R_2 , of grinding wheel is defined as follows:

$$Q_X = -R_2 \sin \alpha, \quad (13)$$

$$Q_Y = P_Y = M_Y, \quad (14)$$

$$Q_Z = P_Z = M_Z, \quad (15)$$

However, when the contact point is defined with respect to the grinding wheel setting angle on left arc, the expression becomes as follows:

$$\delta = \omega - \gamma, \quad (16)$$

$$Q_{X'} = Q_X \cos \delta + Q_Y \sin \delta, \quad (17)$$

The mathematical expression for right arc of the grinding wheel having a radius R_1 can be defined in the same procedures as shown from Eqs. (7)–(17). These formulas were applied to determine the shape of the flute of a microdrill mathematically.

2.2 CAD Model of the Microdrill

The next step is to construct the CAD model of the microdrill. In this study, the CAD model of the microdrill was constructed based on the flute shape of a microdrill that was determined mathematically. Some of the dimensional values of the geometrical features of a microdrill were taken from

Table 2 Geometrical features of the microdrill and their dimensional values

Number	Geometrical features	Value
1	Drill diameter	0.1 mm
2	Web thickness	0.05 mm
3	Point angle	120°
4	Primary face angle	10°
5	Secondary face angle	30°
6	Web taper	0.018 mm/1 mm
7	Helix angle	45°
8	Land thickness	0.042 mm
9	Effective flute length	0.2 mm
10	Flute length	1.8 mm
11	Body length	2.0 mm
12	Flex step length	5.63 mm
13	Flex step diameter	0.7 mm
14	Tape angle	20°
15	Overall length	38.1 mm
16	Shank diameter	3.175 mm

a fabricated microdrill having a 0.1 mm diameter; the values are listed in Table 2, and their corresponding dimensions are depicted in Fig. 4.

3 Constraints and Loads on the Microdrill

During drilling process of the PCB, the microdrill is fixed well, so that the six degrees of freedoms of the shank of the microdrill were fixed as constraints for finite element analysis using the Pro/Mechanica software as shown in Fig. 5.

The loads on the microdrill are the thrust force and the torque. The thrust force can be defined as the force acting along the axis of the microdrill during the drilling process. Thrust force is used to monitor tool wear. This implies that

Fig. 4 Dimensions of a 0.1 mm diameter of CAD model of microdrill: **a** overall model, and **b** side view at section A-A

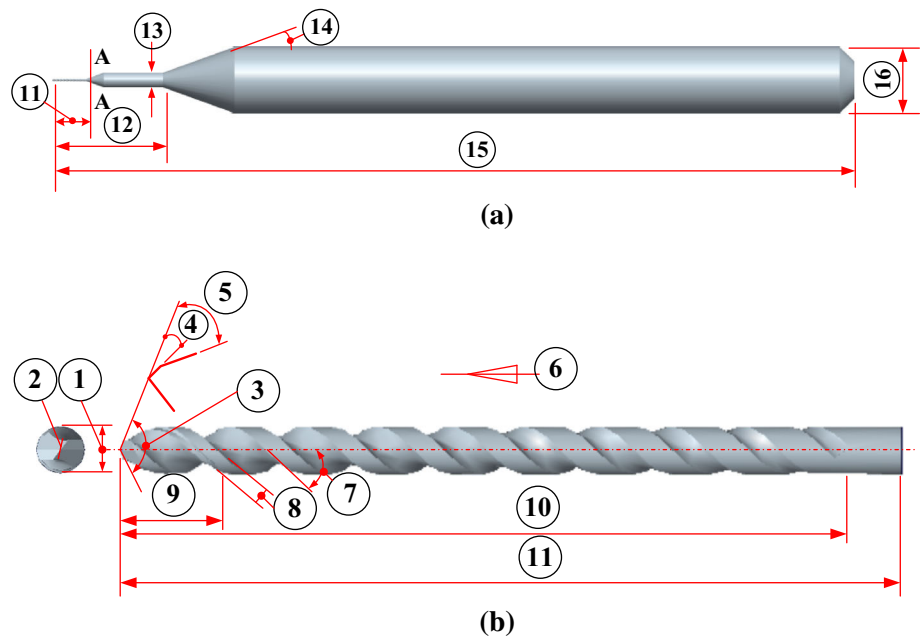


Fig. 5 Constraints of the microdrill

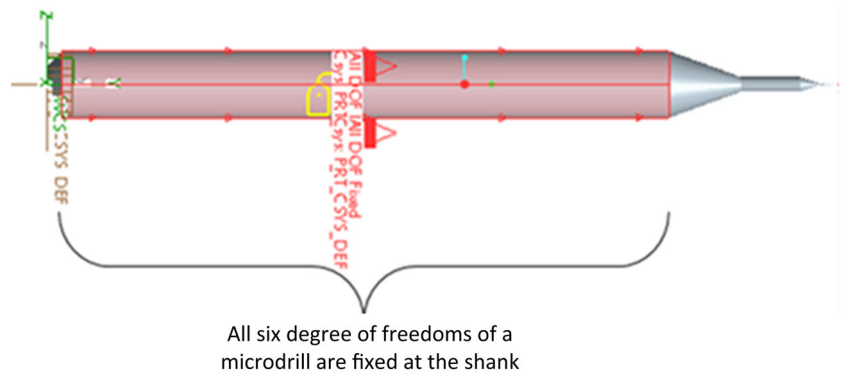


Table 3 Mechanical properties of the microdrill

Material	Tungsten carbide
Density (g/cm ³)	14.4
Young’s modulus (GPa)	590
Poisson’s ratio	0.21
Hardness (HRA)	93.0
Compressive strength (MPa)	5985

it monitors tool life directly. In this study, the material of microdrill is tungsten carbide because of its wear resistance and relatively low cost makes it the ideal material for drilling the PCBs and its mechanical properties are shown in Table 3. The geometric analysis of a microdrill is very complex because the inclination angle, the normal rake angle and the effective rake angle vary radically as we go from the inner most part of the cutting edge to the outer part. The point of the microdrill consists of two parts: the cutting edge and the

chisel edge. The chisel edge does not cut in the usual sense, but it displaces the metal sideways. Jain and Chitale [27] explained that the contribution of chisel edge to total torque M is negligible, but it contributes 50% of the total thrust T , and they derived the formulas of torque and thrust forces based on Fig. 6. For a specific cutting pressure p in kg/mm² and uncut area shown in Fig. 6, it is possible to estimate cutting force F_c in N as follows:

$$F_c = pg \left(\frac{d - c}{2} \right) \left(\frac{f}{2} \right), \tag{18}$$

where g is gravitational acceleration in m/s², d is the diameter in mm of the microdrill, c is chisel edge length in mm, and f is feed in mm/rev.

Based on Fig. 6, the total torque M in mm on a microdrill is expressed as

$$M = \left(\frac{d + c}{2} \right) F_c, \tag{19}$$

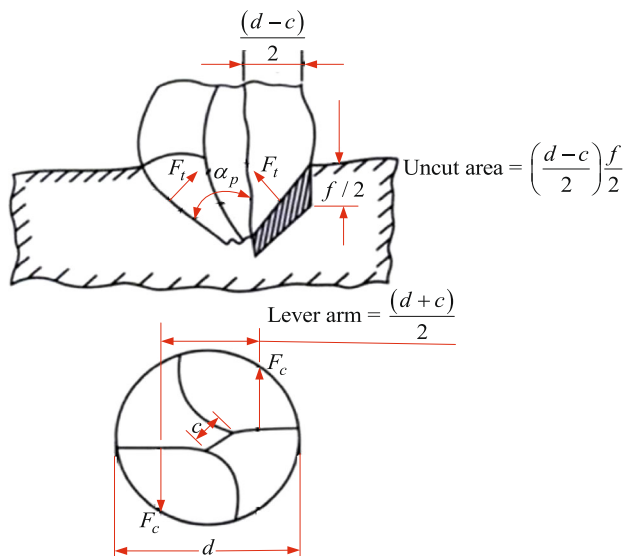


Fig. 6 Cutting action of two fluted twist drill-force system [27]

Substituting Eq. (18) into Eq. (19), the equation of the torque becomes

$$M = pgf \left(\frac{d^2 - c^2}{8} \right), \quad (20)$$

The drill thrust force on each cutting edge is the same; as a result, the drill thrust force T_1 acting on cutting edge according to Fig. 6 is expressed as

$$T_1 = 2F_t \sin \alpha_p, \quad (21)$$

where F_t is the cutting force in N, and α_p is half of the point angle of the microdrill.

The total thrust force T in N on the microdrill is the summation of the drill thrust forces due to cutting edge and chisel edge. Hence, its expression becomes:

$$T = 4F_t \sin \alpha_p, \quad (22)$$

Shaw [28] explained about approximation in the estimation of cutting forces F_c and F_t in terms of the total specific energy since this tends to remain approximately constant for a given work material operating under different cutting conditions. The specific cutting energy will be essentially independent of cutting speed over a wide range of values, provided a large built-up edge (BUE) is not obtained. The workpiece chemistry and structure, effective rake angle and undeformed chip thickness have influence on specific energy. Thus, the cutting force component in the feed f direction is not easily computed, but it is approximated as

$$F_t = \frac{F_c}{2}, \quad (23)$$

In this study, the chip was considered as continuous or spiral during drilling PCB with microdrill at a specific cutting pressure and high spindle speed due to the presence of copper in PCB. Accordingly, when substituting Eq. (18) into Eq. (23), T_1 and T become:

$$T_1 = pgf \left(\frac{d-c}{4} \right) \sin \alpha_p, \quad (24)$$

$$T = pgf \left(\frac{d-c}{2} \right) \sin \alpha_p, \quad (25)$$

The values of thrust forces and torque on the microdrill were calculated using the above formulas.

4 Initial Static Analysis

After the material property was assigned, the constraints were identified and the amounts of loads acting on microdrill were calculated; the next step was initial static analysis. Pro/Mechanica software was used for the initial static analysis, and the results of maximum Von Mises stress were used for finite element analysis or optimization analysis of the control parameters of the model.

5 Configuration of the Design Control Parameters

Some geometric features were calculated indirectly by configuring the design control parameters appropriately. The values of the geometrical features used in determination of the optimal geometric features are shown in Table 4, and the designation of their corresponding design control parameters is indicated in Table 5. In this study, the most important seven geometric features had been considered as control factors, and their corresponding design control parameters' configurations with respect to the original definitions were explained as follows:

Table 4 Values of the ranges of the geometric features

Geometric features	Minimum value	Initial value	Maximum value
Point angle	132°	120°	120°
Primary face angle	8°	10°	13°
Secondary face angle	25°	30°	32°
Web thickness (in mm)	0.048	0.05	0.052
Helix angle	45°	45°	43°
Web taper (in mm/1 mm)	0.015	0.018	0.020
Land thickness (in mm)	0.035	0.042	0.045

Table 5 Geometrical features and their design control parameters

Geometric features	Design control parameters
Point angle	POINT_ANGLE_1
Primary face angle	PRIMARY_FACE_ANGLE_1
Secondary face angle	SECONDARY_FACE_ANGLE_1
Web thickness	P_1_HELIX
Helix angle	PITCH_1
Web taper	X_1_HELIX
Land thickness	R_1_UP

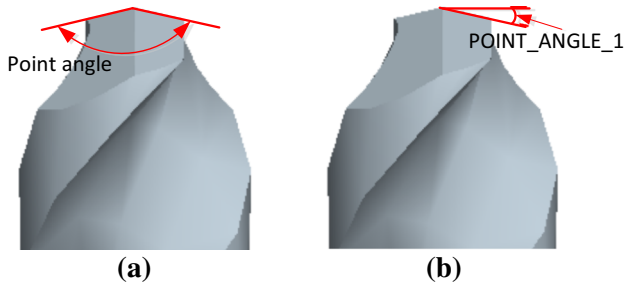


Fig. 7 Point angle definition: **a** Original, and **b** control parameter

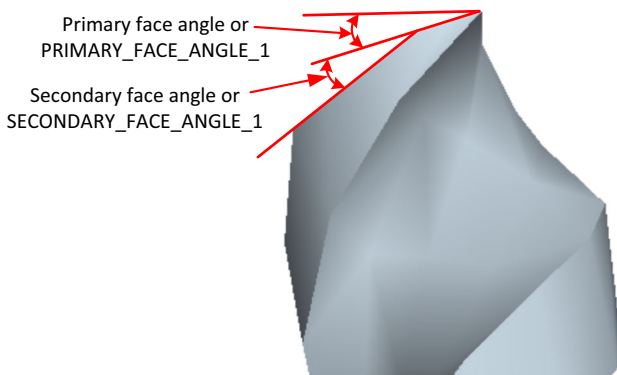


Fig. 8 Definitions of the original and control parameter of primary secondary face angle and primary face angle

5.1 Point Angle

The design control parameter of point angle configuration is shown in Fig. 7, and it was expressed as

$$POINT_ANGLE_1 = 90^\circ - 1/2(\text{Point angle}), \quad (26)$$

5.2 Primary Face Angle

The primary face angle was configured as shown in Fig. 8, and its corresponding expression is

$$PRIMARY_FACE_ANGLE_1 = \text{Primary face angle}, \quad (27)$$

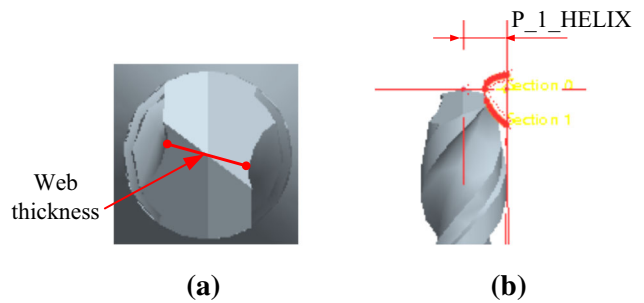


Fig. 9 Web thickness definitions: **a** original and **b** control parameter

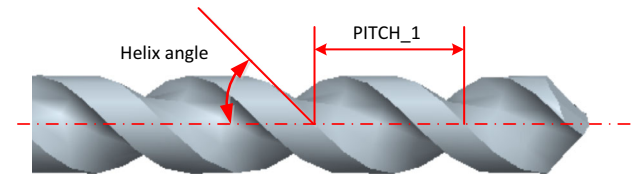


Fig. 10 Definitions of original and control parameter for helix angle

5.3 Secondary Face Angle

The secondary face angle was configured as shown in Fig. 8, and its corresponding expression is

$$SECONDARY_FACE_ANGLE_1 = \text{Secondary face angle}, \quad (28)$$

5.4 Web Thickness

The design control parameter of web thickness configuration is shown in Fig. 9, and it is expressed as:

$$P_1_HELIX = \text{Distance from the center of the flute to axial axis of microdrill.} \quad (29)$$

5.5 Helix Angle

The control parameter of the helix angle of microdrill was obtained from its helix angle θ and the diameter of microdrill d based on the definition shown in Fig. 10 as follows:

$$PITCH_1 = \frac{\pi d}{\tan \theta}, \quad (30)$$

5.6 Web Taper

Web taper of the microdrill depends on the trajectory path of the grinding wheel from central axis of microdrill. Hence, the definition of web taper was seemed as shown in Fig. 11, and it is expressed as

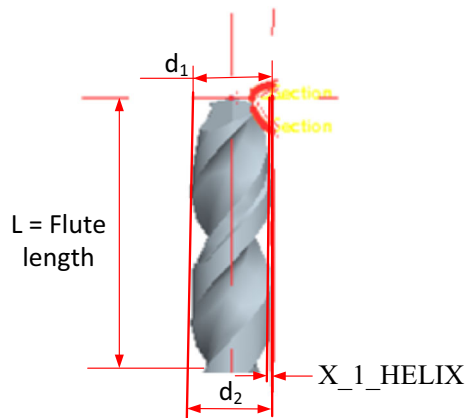


Fig. 11 Definitions of web taper and its control parameter

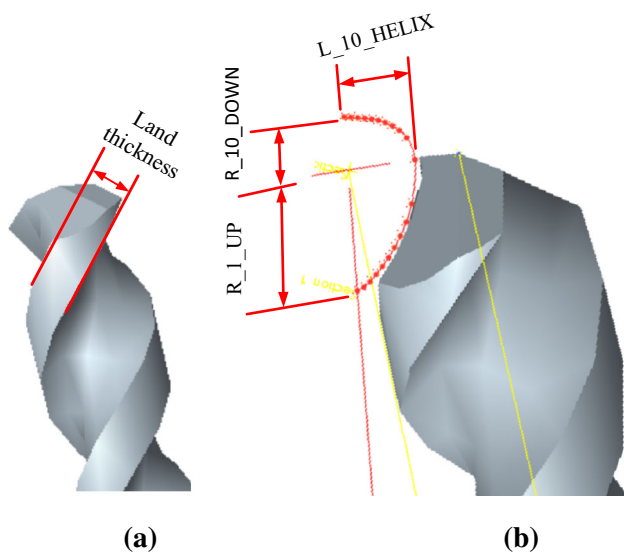


Fig. 12 Land thickness definitions: **a** original and **b** control parameter

$$\text{Web taper} = \frac{d_2 - d_1}{L} = \frac{\Delta d}{L}, \quad (31)$$

Based on Eq. (31) and Fig. 11, the design control parameter of the web taper becomes:

$$X_1_HELIX = \frac{\Delta d}{2}, \quad (32)$$

5.7 Land Thickness

The radius of the grinding wheel affects the land thickness shown in Fig. 12a and the flute. As result, control parameters R_1_UP shown in Fig. 12b were used to control the land thickness.

6 Sensitivity Study Analysis of the Configured Design Control Parameters

Pro/Mechanica software has potential for studying the sensitivity analysis of a model. There are two known sensitivity analysis studies: local sensitivity study analysis and global sensitivity study analysis. Local sensitivity study is useful for comparing the sensitivity of several control parameters. The global sensitivity study analysis provides the sensitivity of a single control parameter to the measures; it is used to know the approximate location of the value in the range of values of the control parameter to minimize the maximum stress. In this study, all the design control parameters were considered in global sensitivity study analysis to determine the value of optimal control parameter in its range that was used to minimize the maximum Von Mises stress.

7 Optimization Analysis of the Geometric Features of the Microdrill

The purpose of the optimization study is to help the designer in optimizing predetermined design control parameters as a function of known measures, such as Von Mises stress or maximum displacement for a specific goal. The optimization analysis was conducted for the ranges of all control parameters that were obtained based on Table 4, Figs. 7, 8, 9, 10, 11, 12 and Eqs. (26)–(32) as a function of Von Mises stress. The objective of this study was to minimize the induced maximum Von Mises stress much smaller than the allowable compressive stress 5985 MPa of the mechanical prosperity of the material of the microdrill and to determine the best optimal geometric features. Hence, the optimal designing that was maximum Von Mises stress is less than allowable compressive stress, that is, $\max_stress_vm < 5.9850e+003$ MPa for determination of the optimal geometric features of the microdrill.

8 Results and Discussion

8.1 Mathematical Determination of the Flute of the Microdrill

The geometry of a microdrill greatly affects the way it behaves during drilling. For instance, less flute space implies reduced amounts of available area to remove drilling debris, which again raises the drilling temperature. On the other hand, larger flute area implies reducing the web thickness and land, and this also leads to reduce the rigidity of the microdrill. In this paper, the flute size was determined mathematically by considering the microdrill and grinding wheel profiles with a setting angle to overcome the above problem. Based on the data of Table 1 and using the mathematical equations from (1) to (17), the mathematical analysis results

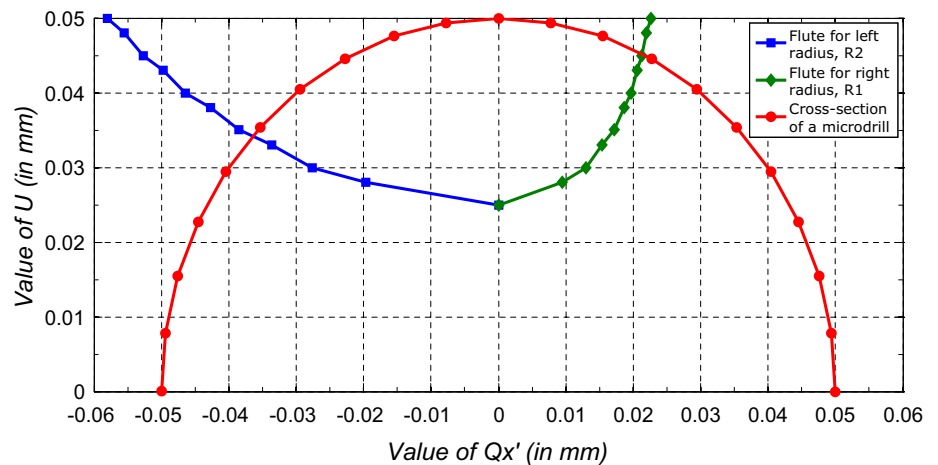
Table 6 Mathematical analysis results of the flute for the left radius R_2

No.	U (mm)	θ_{\min} (rad)	θ_{\max} (rad)	θ_{opt} (rad)	M_y (mm)	M_z (mm)	β (rad)	P_r (mm)	α (rad)	Q_x (mm)	$Q_{x'}$ (mm)
1	0.025	1.570796	1.570796	1.570796	0.000000	0.025000	-2.89E-20	75.00000	0.00000	0.000000	0.0000000
2	0.028	1.141097	2.000496	1.530691	-0.001559	0.027478	-2.08E-05	74.99752	0.25112	-0.019631	-0.0196744
3	0.030	0.985111	2.156482	1.508323	-0.002649	0.029941	-3.53E-05	74.99506	0.35556	-0.027501	-0.0276192
4	0.033	0.877636	2.263956	1.487617	-0.003819	0.032388	-5.09E-05	74.99261	0.43591	-0.033356	-0.0335732
5	0.035	0.795603	2.345990	1.477773	-0.004598	0.034849	-6.13E-05	74.99015	0.50467	-0.038198	-0.0384734
6	0.038	0.729728	2.411865	1.458654	-0.005935	0.037264	-7.91E-05	74.98774	0.56469	-0.042277	-0.0426850
7	0.040	0.675132	2.466461	1.451374	-0.006739	0.039715	-8.99E-05	74.98529	0.62024	-0.045917	-0.0463965
8	0.043	0.628875	2.512718	1.432648	-0.008277	0.042095	-1.10E-04	74.98291	0.67034	-0.049079	-0.0497216
9	0.045	0.589031	2.552562	1.426804	-0.009132	0.044534	-1.22E-04	74.98047	0.71859	-0.052007	-0.0527326
10	0.048	0.554262	2.587331	1.408151	-0.010878	0.046873	-1.45E-04	74.97813	0.76247	-0.054566	-0.0554847
11	0.050	0.523599	2.617994	1.389282	-0.012765	0.049179	-1.70E-04	74.97582	0.80383	-0.056881	-0.0580130

Table 7 Mathematical analysis results of the flute for the right radius R_1

No.	U (mm)	θ_{\min} (rad)	θ_{\max} (rad)	θ_{opt} (rad)	M_y (mm)	M_z (mm)	β (rad)	P_r (mm)	α (rad)	Q_x (mm)	$Q_{x'}$ (mm)
1	0.025	1.570796	1.570796	1.570796	0.000000	0.025000	-2.89E-20	75.00000	0.00000	0.000000	0.0000000
2	0.028	1.141097	2.000496	1.473398	-0.003782	0.027370	-5.04E-05	74.99763	0.51170	0.009059	0.0094520
3	0.030	0.985111	2.156482	1.414614	-0.006599	0.029635	-8.80E-05	74.99537	0.72351	0.012247	0.0129604
4	0.033	0.877636	2.263956	1.358227	-0.009697	0.031768	-1.29E-04	74.99323	0.88386	0.014304	0.0153792
5	0.035	0.795603	2.345990	1.302063	-0.013142	0.033744	-1.75E-04	74.99126	1.01523	0.015718	0.0172021
6	0.038	0.729728	2.411865	1.245583	-0.016945	0.035534	-2.26E-04	74.98947	1.12555	0.016696	0.0186369
7	0.040	0.675132	2.466461	1.093108	-0.026006	0.035522	-3.47E-04	74.98948	1.12468	0.016689	0.0197343
8	0.043	0.628875	2.512718	0.993085	-0.032823	0.035603	-4.38E-04	74.98940	1.12934	0.016726	0.0206019
9	0.045	0.589031	2.552562	0.903196	-0.039399	0.035339	-5.25E-04	74.98967	1.11331	0.016598	0.0212754
10	0.048	0.554262	2.587331	0.838891	-0.044892	0.035335	-5.99E-04	74.98968	1.11291	0.016594	0.0219416
11	0.050	0.523599	2.617994	0.788889	-0.049825	0.035479	-6.64E-04	74.98954	1.12133	0.016663	0.0226105

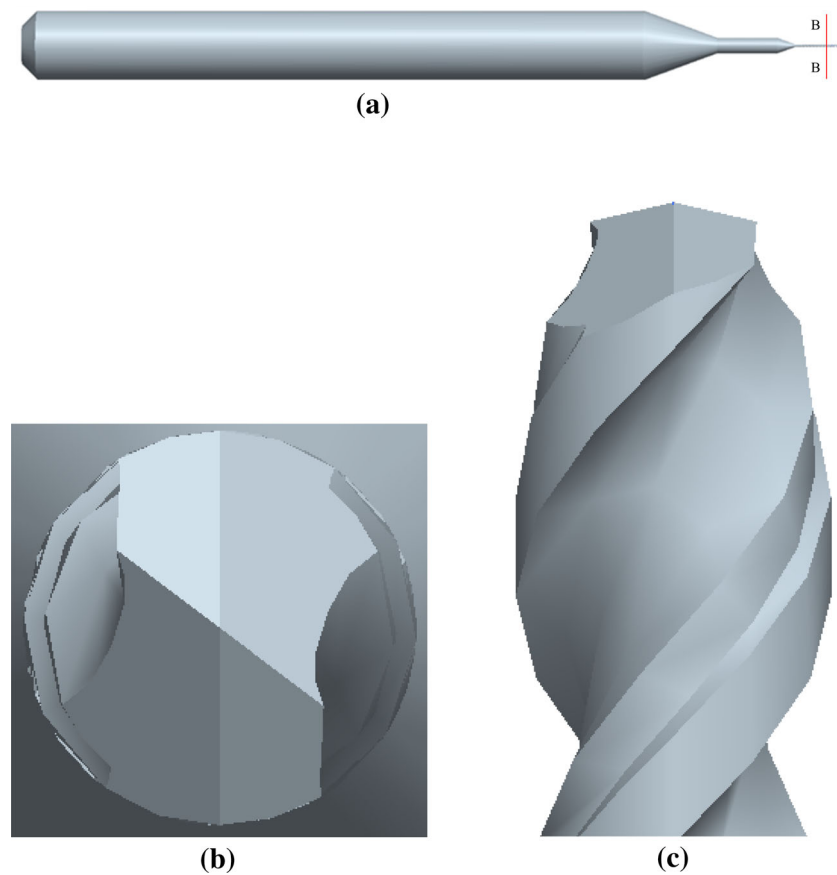
Fig. 13 Flute of the microdrill



of the flute corresponding to the left radius R_2 and right radius R_1 of the grinding wheel profile during cutting of the microdrill are shown in Tables 6 and 7, respectively. These results are the values of contact points with respect to grinding wheel setting angle during the cutting of microdrill, and they were used to construct the flute of a microdrill. The

consideration of grinding wheel setting angle is important to get accurate shape of the flute. Based on Tables 6 and 7, the shape of the flute of a 0.1 mm diameter of microdrill was drawn and its profile is shown in Fig. 13. This shape makes the construction of CAD model and fabrication of microdrill easier.

Fig. 14 The constructed 3D solid CAD model of the microdrill using Pro/Engineer software: **a** overall shape, **b** top view, and **c** front view at section B-B



8.2 CAD Model of the Microdrill

After determining the flute of a 0.1 mm diameter of microdrill, the next step was to construct the 3D CAD model of a 0.1 mm diameter of a microdrill, as shown in Fig. 14. It was constructed using Pro/Engineer Wildfire 5.0 software based on the flute shape of the microdrill shown in Fig. 13 and the dimensional values of the geometrical features of the microdrill, as shown in Table 2. Its chisel edge length is 0.066 mm. The flute shape was defined under “Insert” toolbar by pointing at “Helical Sweep” and then selecting “Cut” function in Pro/Engineer Wildfire 5.0 software during the construction of microdrill. This constructed CAD model of microdrill has an appropriate flute area that is capable of removing the drilling debris easily; in addition, the cutting and chisel edges become good as shown in Fig. 13. The land is the area remaining after fluting. The CAD model is used to construct the margin relieved for certain length called effective flute length to reduce the amount of land that creates friction with the hole wall (thus generating heat). The amount of land remaining in contact with the hole wall during drilling is referred to as the margin. The wider the margin, the greater the friction area and the higher the drilling temperature, resulting in higher extents of heat-related hole quality defects such as resin smear

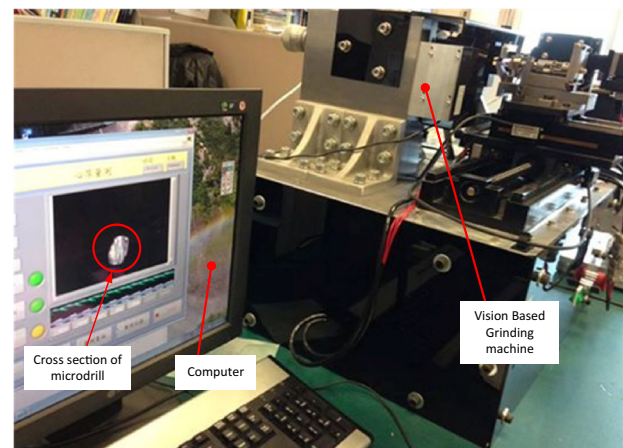
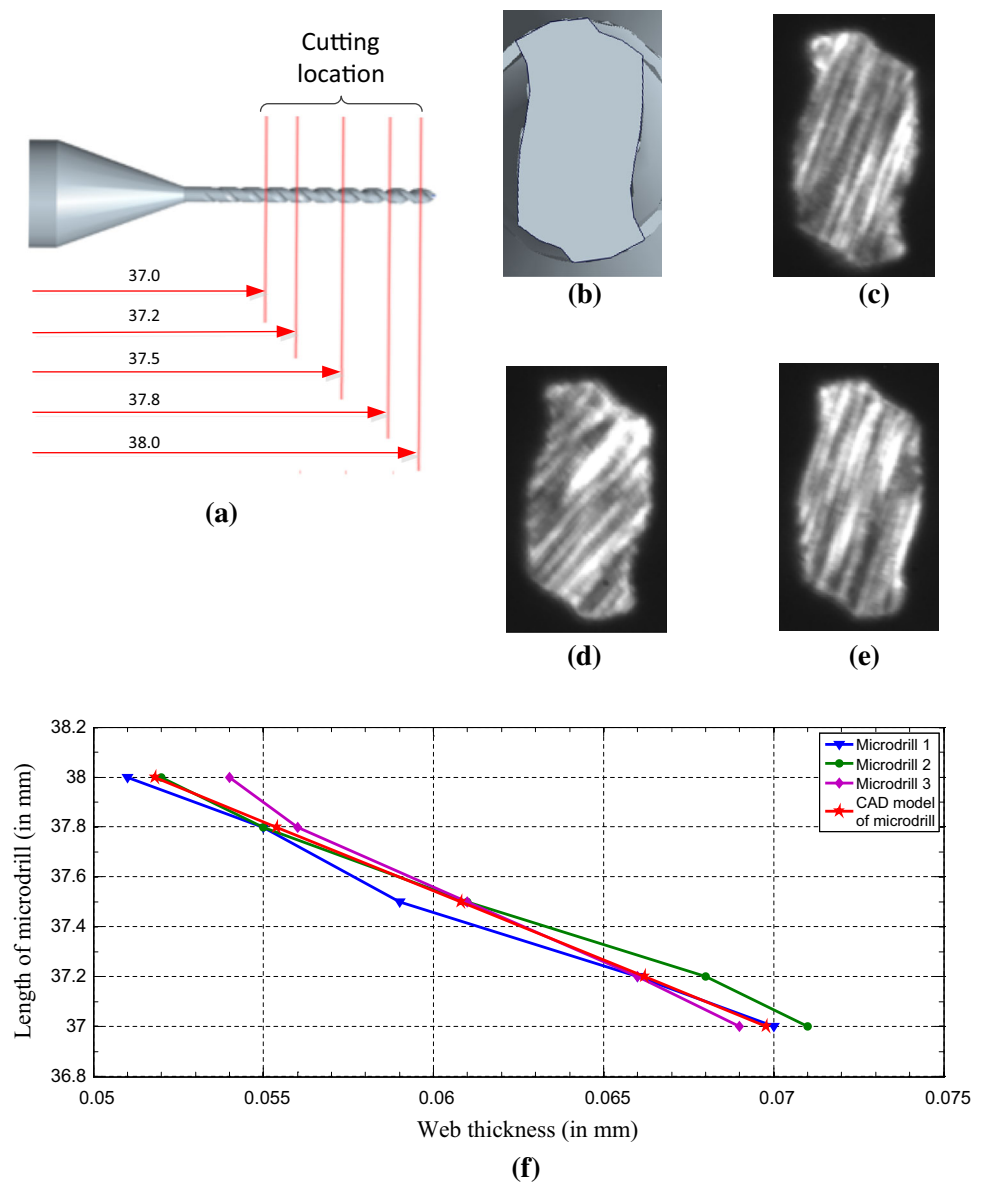


Fig. 15 Grinding machine for measuring web thickness

and plowing (defined as furrows in the resin). There are common drill point defects, such as cutting edge becomes hook or layback, flank areas overlap or have a certain gap along chisel edge, and flare and negative of flank areas. These defects can also be solved during mass production of microdrills as long as the flute is determined by considering both definition of microdrill and grinding wheel profile for a certain helix angle and setting angle as it is stated in this paper.

Fig. 16 Illustration of web thickness: **a** cutting location on microdrill, **b** cross section of model at 38.0 mm length, **c** cross section of fabricated microdrill 1 at 38.0 mm length, **d** cross section of fabricated microdrill 2 at 38.0 mm length, **e** cross section of fabricated microdrill 3 at 38.0 mm length and **f** web thickness results



8.3 Cross-sectional Comparison Between the CAD Model of the Microdrill and the Fabricated Microdrill

After the overall CAD model of the 0.1 mm diameter of the microdrill was constructed, the next task was the cross-sectional comparison between the CAD model and the fabricated microdrill, to verify the validation of the constructed CAD model. The cross-sectional comparison between the model and a fabricated 0.1 mm diameter of microdrill was carried out by cutting both of them at different lengths. After cutting the model and microdrills, the cross-sectional shapes of the flutes and the measured web thicknesses were taken as criteria for comparison. The vision-based grinding machine, which shows its setup in Fig. 15, was used to cut the

three fabricated microdrills using destructive method and to measure their web thickness automatically, whereas the “View Manager” function under “View” toolbar was used to cut the CAD model and “Measure” function under “Analysis” toolbar was used to measure its web thickness using Pro/Engineer Wildfire 5.0 software. The flute and web thickness of the constructed CAD model of microdrill were compared with a fabricated microdrill by cutting both of them at different lengths as shown in Fig. 16a. For example, the flute shapes of the model and fabricated microdrills after cutting at 38.0 mm length are approximately the same as shown in Fig. 16b–e. After cutting the microdrills for different lengths, the web thickness was measured and the results are depicted in Fig. 16f. According to Fig. 16f, the web thicknesses of the model and the fabricated microdrills are almost the same.

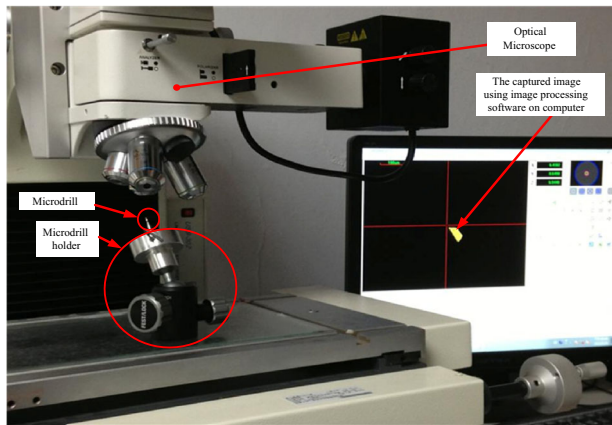


Fig. 17 Image capturing setup

Hence, the web taper of a model is approximately the same as that of the fabricated drill. Besides, the comparison on the shapes of cutting edge, chisel edge, primary flank areas and secondary flank areas of the model with fabricated 0.1 mm diameter of microdrill was carried out by taking images from fabricated microdrill using optical microscope and QIM3008_V2.7 image processing software at certain inclination angle as shown in Fig. 17. The taken images are listed in Table 8. Based on the shapes of the model in Fig. 18 and Table 8, the cutting edge, chisel edge, primary flank areas and secondary flank areas are also almost the same as the fabricated microdrills. According to these comparisons results, the developed approach that was used to determine the flute of a microdrill mathematically by defining the undercutting relative positions of both the microdrill and grinding wheel and their profiles with respect to setting angle and to construct 3D CAD model of the 0.1 mm diameter of microdrill, is effective.

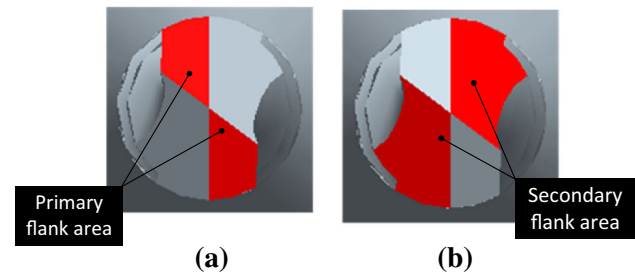


Fig. 18 CAD model shapes of a microdrill: **a** primary flank area and **b** secondary flank area

8.4 Loads on the Microdrill

The calculation of the loads acting on the microdrill during drilling printed circuit boards is necessary to predict the possibility of failure of a microdrill and preserve the quality of the drilled hole as much as possible good. In addition to this, it is also used as the first step for determination of the optimal geometric features of the microdrill using finite element analysis method. In this study, microdrill of 0.1 mm diameter with a 0.066 mm of chisel edge length was required to drill printed circuit board at 0.01 mm/rev of a maximum feed and 100 kg/mm² of drilling/cutting pressure using CNC drilling machine PK-2630/S1. Therefore, it is possible to calculate the amount of thrust force and torque acting on the microdrill for the above-selected criterions. Based on the dimensional values listed in Table 2, the loads acting on the microdrill that include the drill thrust force due to cutting edge T_1 , the total thrust force T , and the drill torque M were calculated using Eqs. (18)–(25). For gravitational acceleration of 9.80665 m/s², the calculated results are $T_1 = 0.072189$ N, $T = 0.144378$ N, and $M = 0.006919$ Nmm, respectively. According to these results, the drill thrust force due to cut-

Table 8 Captured images of a 0.1 mm diameter of microdrills


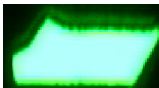

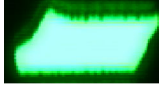

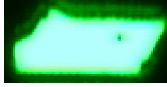
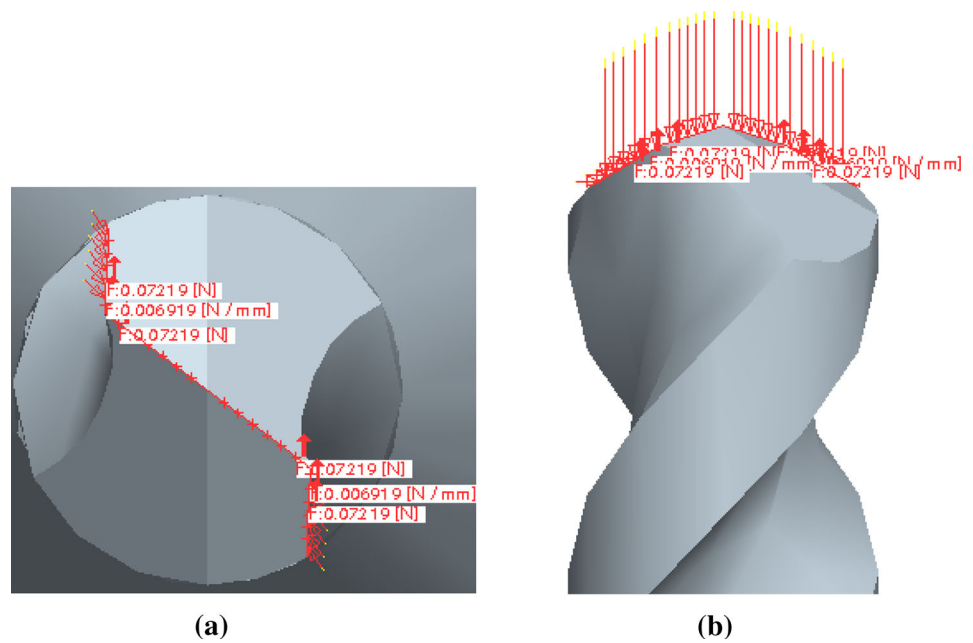
Sample Image	Shape of primary flank area	Shape of secondary flank area
1		
2		
3		

Fig. 19 Distribution of the thrust forces and torque on the microdrill: **a** top view and **b** side view



ting edge is 0.072189 N, the total thrust force due to both the chisel and cutting edges is 0.144378 N and the total torque due to cutting edge is 0.006919 Nmm. Hence, thrust force due to chisel edge becomes 50 % of 0.144378 N according to the previous explanation in chapter 3.

Pro/Mechanica is a product of Parametric Technology Corporation (PTC) and works with Pro/Engineer software in integrated mode. Pro/Mechanica structure is a finite element analysis (FEA) tool that allows one to solve for stresses and deflections analysis in structural elements. Therefore, the FEA analysis was carried out on this model, first by defining and assigning material properties of the solid model, and adding constraints and the calculated loads on the model using Pro/Mechanica structure. The recommended material of the microdrill is tungsten carbide as it was explained before in chapter 1, and its material properties shown in Table 3 were defined and assigned to CAD model of this microdrill. The microdrill does not have any motion during printed circuit board drilling process; hence, the six degrees of freedoms of the shank of the microdrill were fixed as constraints as shown in Fig. 5 on the model. The next step was to add the calculated results of loads on the simplified model corresponding to their edges. After the loads were added on the model using Pro/Mechanica software, the distributions of the results of thrust force on the cutting edge, thrust force on the chisel edge, and the torque along the cutting edge of the microdrill are shown in Fig. 19.

8.5 The Initial Static Analysis

The major advantage of using Pro/Mechanica is the following: Instead of constantly refining and recreating finer and

finer meshes, convergence is obtained by increasing the order of the interpolating polynomials on each element. The mesh stays the same for all iterations, called a p-loop pass. The use of higher-order interpolating polynomials for convergence analysis leads to the p-element class of FEA methods, where the “p” denotes polynomial. Its automatic mesh generators are much more effective with p-elements, due to the reduced requirements and limitations on mesh geometry. Hence, the CAD model was transferred into Pro/Mechanica where the material properties were assigned, loads and constraints were applied, and the mesh was automatically generated. Then, the initial static stress analysis was run on the model. The maximum Von Mises stress acting on the edges was about 7951.113 MPa, and the maximum displacement was about 3.685058×10^{-4} mm based on the simulation results, as shown in Fig. 20. In order to confirm that the designed model is safe for the calculated load results during the PCB drilling process, the maximum Von Mises stress must be less than the allowable compress stress of the material of the assigned material. However, the maximum Von Mises stress 7951.113 MPa was greater than the allowable compress stress 5985 MPa depicted in Table 3. This implied that the microdrill was failed for the initial values of geometric features for drilling printed circuit board at 0.01 mm/rev of a maximum feed and 100 kg/mm² of drilling/cutting pressure using CNC drilling machine. Hence, the optimization analysis must be run for the given design control parameters. The initial static stress analysis results were used as the basis for the optimizations analysis or finite element analysis (FEA) to determine the best design values of the geometric features of a microdrill.

Fig. 20 Initial static analysis results: **a** stress distribution and **b** displacement distribution

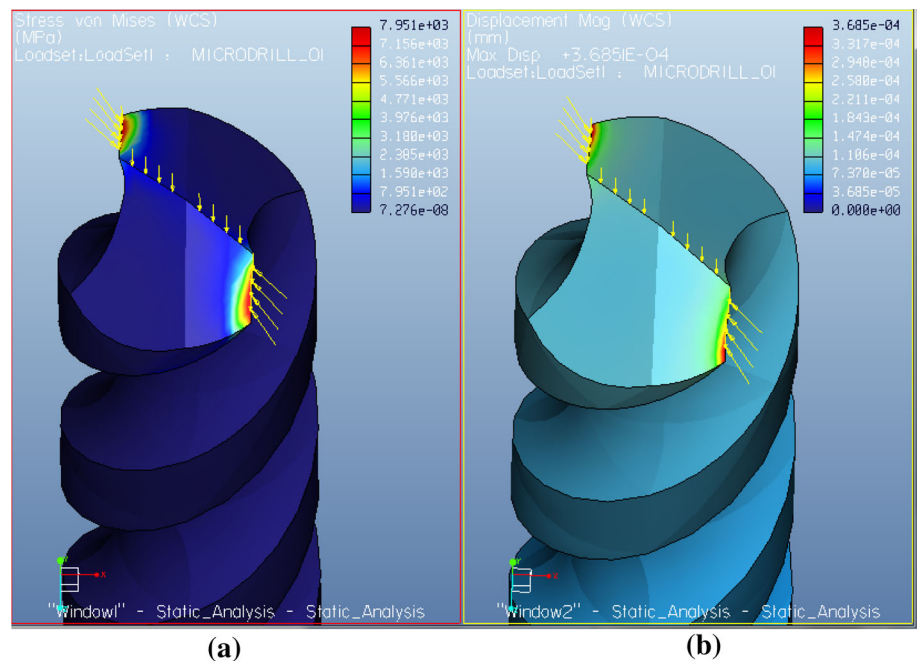


Table 9 Values of the ranges of the control parameters

Control parameters	Minimum value	Initial value	Maximum value
POINT_ANGLE_1	24°	30°	30°
PRIMARY_FACE_ANGLE_1	8°	10°	13°
SECONDARY_FACE_ANGLE_1	25°	30°	32°
P_1_HELIX (in mm)	0.048	0.05	0.052
PITCH_1 (in mm)	0.314	0.314	0.337
X_1_HELIX (in mm)	0.0135	0.0162	0.018
R_1_UP (in mm)	0.0560	0.0580130	0.0593

8.6 Configuration of the Design Control Parameters

The design control parameters were set for each geometric feature to handle easily the optimization analysis of the geometric features of the microdrill with respect to their actual values. The values of the ranges of geometric features were taken reasonably, and they were calculated indirectly by configuring the design control parameters appropriately. The minimum and maximum values of the geometric features were defined in terms of their corresponding control parameters. For example, the minimum and maximum geometric values of helix angle are 45° and 43°, respectively, because the control parameter value (pitch value) of 45° is 0.314 mm whereas 43° is 0.337 mm. The name of the control parameters was also written as simple as in ways of compatibility of the software. The results of the design control parameters of the geometric features shown in Table 9 were obtained based on Tables 4, 5, Figs. 7, 8, 9, 10, 11, 12 and Eqs. (26)–(32). The ranges of these control parameter values were used to know the sensitivities of the geometric features

for maximum Von Mises stress on the model and to determine the best design value within the ranges.

8.7 Sensitivity Analysis of the Configured Design Control Parameters

A global sensitivity study is used to analyze the changes in product performance measures when a design control parameter (or a combined change with more than one design control parameters) is varied over a prescribed control parameter range. Pro/Mechanica provides this analysis by calculating performance measure values at numerous designs in the ranges of design control parameters. Design control parameters are perturbed a number of times (default is 10 in Pro/Mechanica) with a uniform design perturbation (or design interval). Pro/Mechanica automatically changes the solid model (if fully parameterized), updates finite element mesh and analyzes the finite element model for each design change. This computation is usually very expensive (i.e., time consuming) for large-scale models. The results of the global

sensitivity study can be shown in a graph of a measure versus a design control parameter. In this study, all design control parameters of the geometric features of the microdrill were selected for global sensitivity study analysis because the determination of optimal control parameters would be more accurate even it takes much time to find the best design value for all geometric features. The global sensitivity graphs of the design control parameters of the geometric features for maximum Von Mises stress that were drawn based on Table 9 are shown in Fig. 21. According to Fig. 21, as the values of the design control parameters of point angle, helix angle, web taper, and land thickness increase, the induced stress decreases, whereas as the values of the design control parameters of primary face angle, secondary face angle, and web thickness increase, the induced stress increases. Based on these results, the optimization analysis was used to find the best design values in order to reduce the stress.

8.8 Optimization Analysis of the Geometric Features of the Microdrill

The optimization analysis was conducted using Pro/Mechanica for the ranges of all control parameters tabulated in Table 9 by taking consideration of the global study analysis results to minimize the maximum Von Mises stress acting on the model. In this analysis, the design limit was the maximum Von Mises stress acting on the model must be less than the allowable compress stress 5985 MPa of the material of a microdrill. The optimization analysis determined the best design values of all control parameters of the geometric features of the microdrill that were used to minimize the maximum Von Mises stress from 7951.113 to 5062.8 MPa. Meanwhile, the magnitude of the maximum displacement was minimized from 3.685058×10^{-4} mm to 2.817×10^{-4} mm, the results of the best design found depicted in Table 10, and the distributions of stress and displacement on the optimized model are shown in Fig. 22. Based on the best design values of optimization analysis results shown in Table 10, the optimal geometric features of a 0.1 mm diameter of microdrill are point angle of 120° (POINT_ANGLE_1 of 30°), primary face angle of 8° (PRIMARY_FACE_ANGLE_1 of 8°), secondary face angle of 25° (SECONDARY_FACE_ANGLE_1 of 25°), web thickness of 0.0488 mm (P_1_HELIX of 0.0488471 mm), helix angle of 44° (PITCH_1 of 0.325 mm), web taper of 0.018 mm/1 mm (X_1_HELIX of 0.0162 mm) and land thickness of 0.042 mm (R_1_UP of 0.0580130 mm). According to the global sensitivity graph, Fig. 21, the best design values of the control parameters are reasonable because when the primary face angle, secondary face angle, and web thickness decrease, and helix angle increases, the maximum Von Mises stress decreases. Based on this optimization analysis, the initial values of geometric features of primary face angle were changed from 10° to 8° , secondary face angle

was changed from 30° to 25° , helix angle was changed from 45° to 44° , and the web thickness was changed from 0.05 to 0.0488471 mm, but other geometric features were the same as their own initial values. Accordingly, the optimal geometric features were successfully determined, and the design of a 0.1 mm diameter of microdrill became safe for drilling printed circuit board at maximum feed of 0.01 mm/rev and cutting pressure of 100 Kg/mm². Therefore, the determination of optimal geometric features of a microdrill by setting design control parameters for geometric features and carrying out optimization of the stress/displacement analysis using Pro/Mechanica software is a useful approach.

9 Conclusions

In this paper, the effective method was investigated to determine mathematically the shape of flute of a 0.1 mm diameter of microdrill. The flute shape was determined mathematically by defining the undercutting relative positions of both the microdrill and grinding wheel and their profiles with respect to grinding wheel setting angle. The contact points of the grinding wheel during cutting or fluting of microdrill were analyzed mathematically with respect to grinding wheel setting angle, and these values were used to plot the flute shape for the left and right radii of grinding wheel. The large flute area and small flute area have their own advantages and disadvantages on the strength of the microdrill. As a result, this approach is effective to determine the appropriate flute for a given microdrill and grinding wheel. In addition, it is possible to construct easily the CAD model of a microdrill. The 3D CAD model of a 0.1 mm diameter of microdrill has also been constructed based on this mathematically determined flute shape using Pro/Engineer Wildfire 5.0 software. In order to reduce the contact area of the land of a microdrill with the hole wall, the margin was relieved for the effective flute length.

After the 3D CAD model of the 0.1 mm diameter of microdrill had been constructed, the cross-sectional comparison between the model and a fabricated 0.1 mm diameter of microdrill has been carried out, to verify the validation of the constructed CAD model. The flute and web thickness of the model and a fabricated 0.1 mm diameter of microdrill were used for the purpose of comparison. The flute and web thickness of the constructed CAD model of microdrill were compared with a fabricated microdrill by cutting both of them at different lengths using a vision-based grinding machine. After cutting the microdrills for different lengths, the flute shapes at different cross sections were taken and the web thicknesses were also measured. Consequently, the flute shapes and web thickness were compared, and results indicated that the model and the fabricated microdrills have almost the same flute shape and web thickness. Consequently,

Fig. 21 Global sensitivity analysis graphs: **a** point angle, **b** primary face angle, **c** secondary face angle, **d** web thickness, **e** helix angle, **f** web taper and **g** land thickness

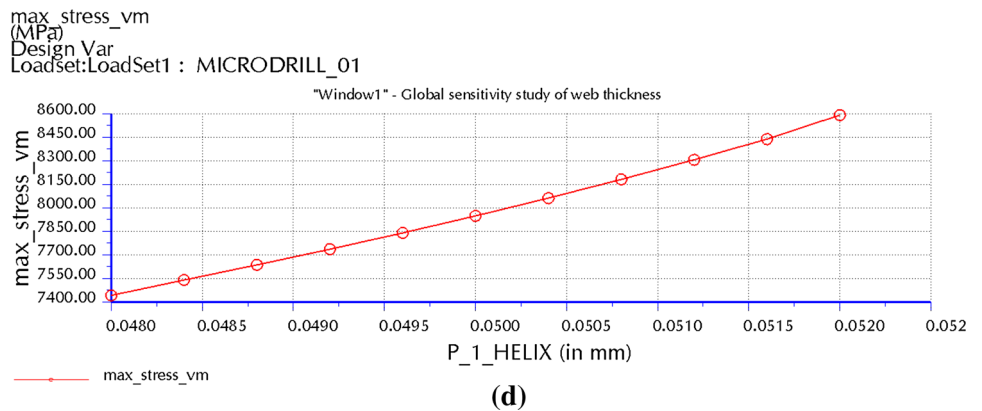
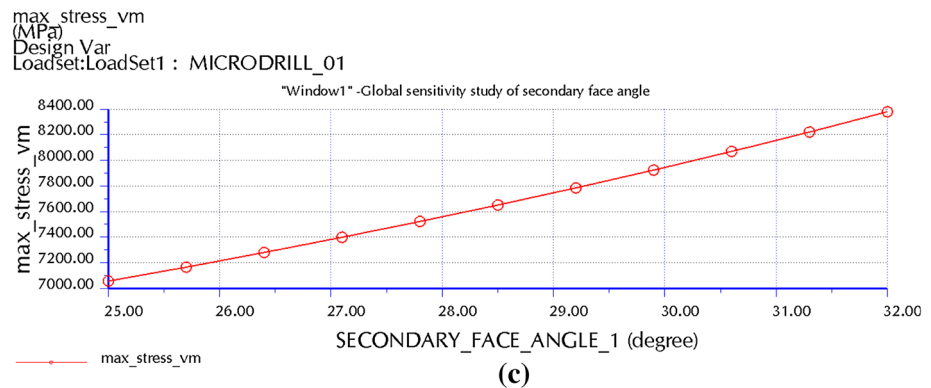
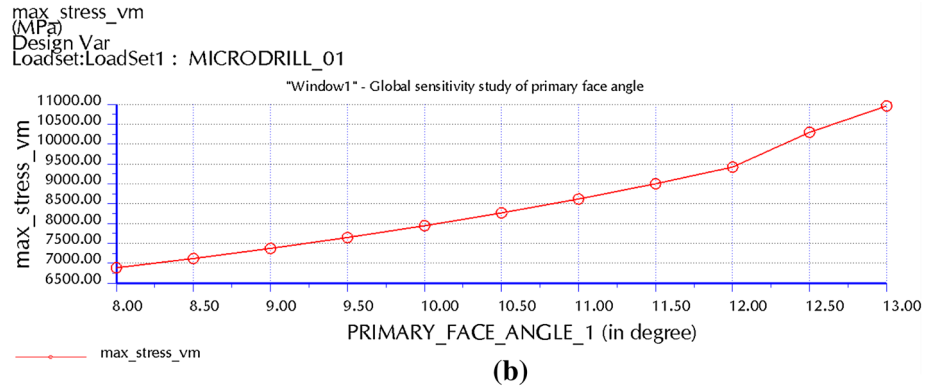
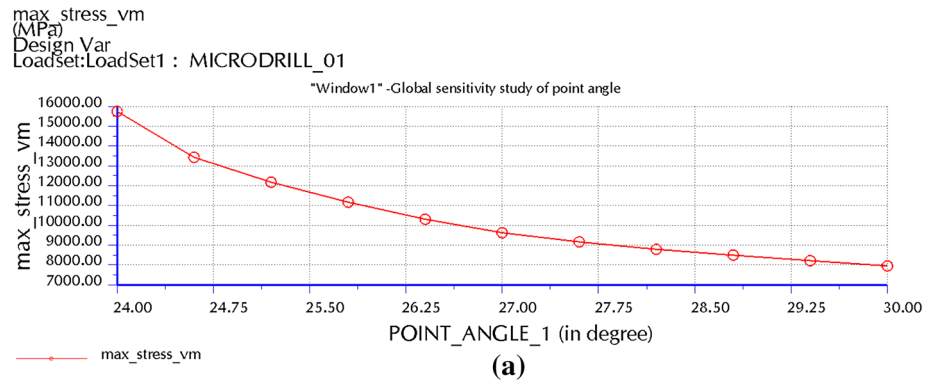
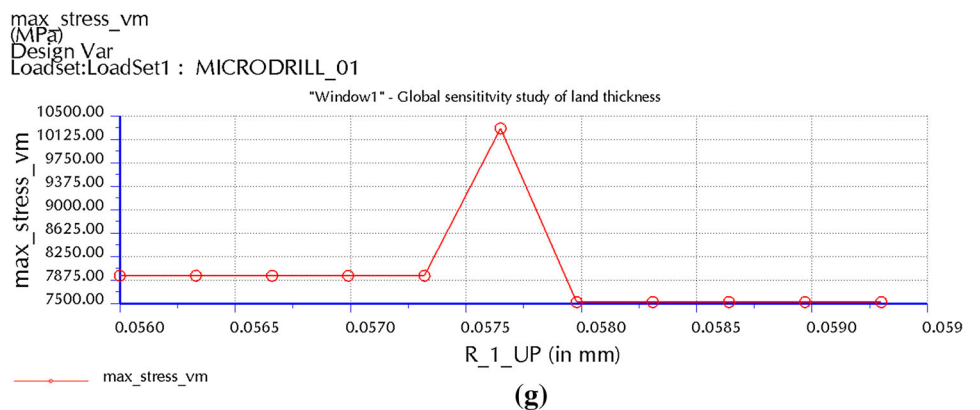
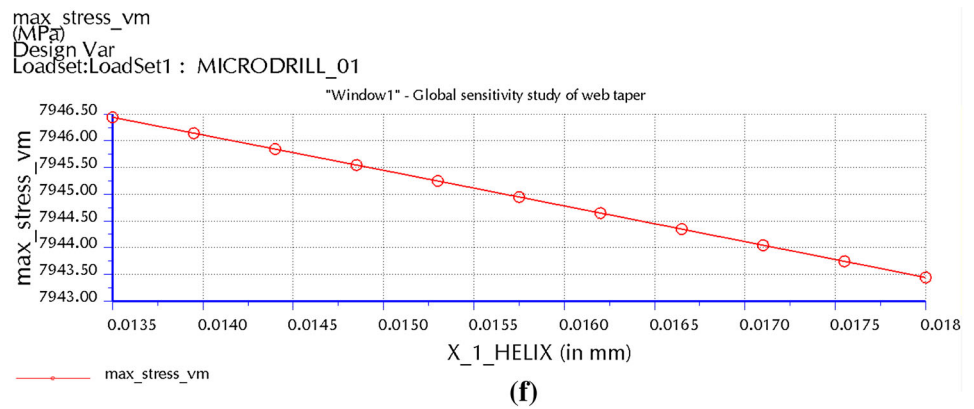
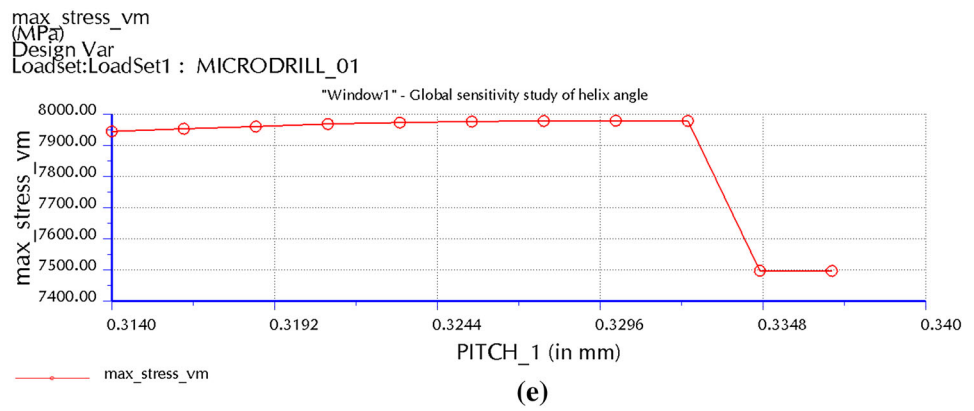


Fig. 21 continued



the web taper of a model is approximately the same as that of the fabricated drill. Besides, the comparison on the shapes of cutting edge (lip), chisel edge, primary flank areas and secondary flank areas of the model with fabricated microdrill was carried out by taking microdrill’s images using an optical microscope. Based on the shapes of the model, the cutting edge, chisel edge, primary flank areas and secondary flank areas are also almost the same as the fabricated microdrills. According to these comparisons results, the approach that was used to determine the flute of a microdrill mathematically by defining the undercutting relative positions of

both the microdrill and grinding wheel and their profiles with respect to setting angle, and then to construct 3D CAD model of the 0.1 mm diameter of microdrill, is effective.

The optimal geometrical features of a 0.1 mm diameter of microdrill that was required to drill printed circuit board at 0.01 mm/rev of a maximum feed and 100 kg/mm² of drilling/cutting pressure using CNC drilling machine PK-2630/S1 have been determined. The determination of the optimal geometric features was carried out, firstly, the amount of thrust forces and torque acting on the edges microdrills was calculated for the mentioned drilling criterions; sec-

Fig. 22 Optimization analysis results: **a** stress distribution and **b** displacement distribution

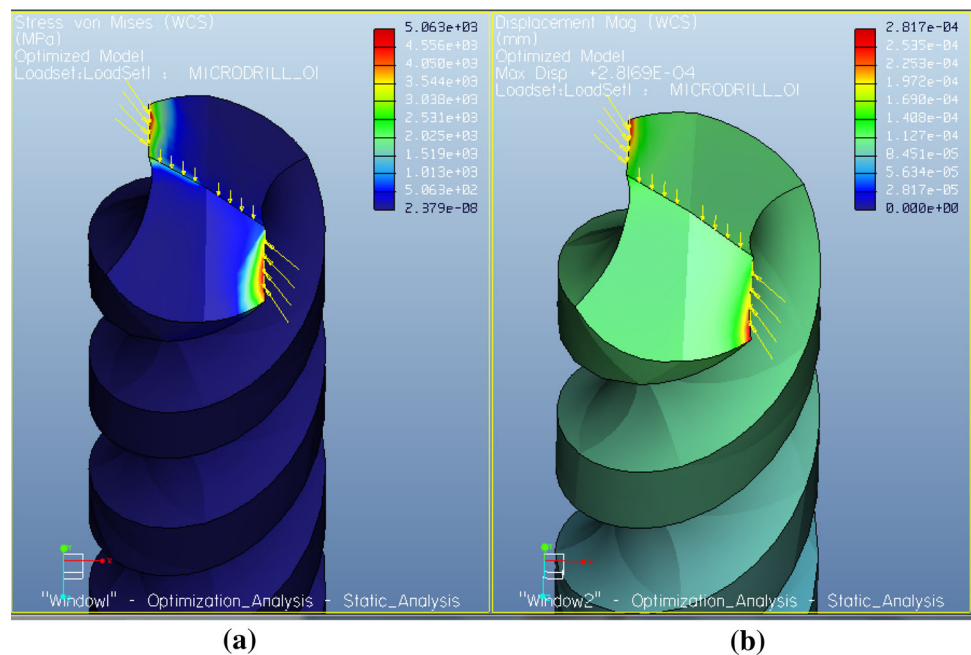


Table 10 Best design found

Control parameters	Value found
POINT_ANGLE_1	30°
PRIMARY_FACE_ANGLE_1	8°
SECONDARY_FACE_ANGLE_1	25.0794° ≈ 25°
P_1_HELIX	0.0488471 mm
PITCH_1	0.325 mm
X_1_HELIX	0.0162 mm
R_1_UP	0.0580130 mm

only, the Pro/Mechanica software was used to assign the material properties and to add the constraints and loads on the 3D CAD model of a microdrill. After that, the initial static stress analysis was run; the maximum induced Von Mises stress acting on microdrill was about 7951.113 MPa, and the magnitude of the maximum displacement was about 3.685058×10^{-4} mm as initial static analysis results. According to the initial results, the designed microdrill was failed to drill PCB at 0.01 mm/rev of feed and 100 Kg/mm² cutting pressure because the maximum induced Von Mises stress, 7951.113 MPa, was greater than the allowable compress stress 5985 MPa for the initial design values of the microdrill. The optimization analysis has been carried out using Pro/Mechanica by setting design control parameters for geometric features to determine the optimal geometric features. Based on this analysis results, the optimal geometric features of the 0.1 mm diameter of microdrill have been set as follows: Point angle was 120°, primary face angle was changed from 10° to 8°, secondary face angle was changed from 30°

to 25°, web thickness is changed from 0.05 mm to 0.0488471 mm, helix angle was changed from 45° to 44°, web taper was 0.018 mm/1 mm, and land thickness was 0.042 mm. For the best design values, the maximum induced Von Mises stress was minimized from 7951.113 to 5062.8 MPa. Meanwhile, the magnitude of the maximum displacement was minimized from 3.685058×10^{-4} mm to 2.817×10^{-4} mm on the microdrill. Therefore, the determination of optimal geometric features of a microdrill by setting design control parameters for geometric features and carrying out optimization of the stress/displacement analysis using Pro/Mechanica software is a useful approach.

References

1. Coombs, C.: Printed Circuits Handbook. McGraw-Hill, New York (2007)
2. Zheng, L.J.; Wang, C.Y.; Fu, L.Y.; Yang, L.P.; Qu, Y.P.; Song, Y.X.: Wear mechanisms of micro-drills during dry high speed drilling of PCB. *J. Mater. Process. Technol.* **212**(10), 1989–1997 (2012). doi:10.1016/j.jmatprotec.2012.05.004
3. Khorasani, A.M.; Asadnia, M.; Saadatkia, P.: Modeling of TiC-N thin film coating process on drills using particle swarm optimization algorithm. *Arab. J. Sci. Eng.* **38**(6), 1565–1571 (2013)
4. Uysal, A.: A study on drilling of AISI 304L stainless steel with nanocomposite-coated drill tools. *Arab. J. Sci. Eng.* **39**(11), 8279–8285 (2014)
5. Hsieh, J.F.: Mathematical modeling of a complex helical drill point. *J. Manuf. Sci. Eng. Trans. ASME* **131**(6), 0610061–06100611 (2009)
6. Hsieh, J.-F.; Lin, P.D.: Drill point geometry of multi-flute drills. *Int. J. Adv. Manuf. Technol.* **26**(5-6), 466–476 (2005). doi:10.1007/s00170-003-2027-x

7. Radhakrishnan, T.; Wu, S.M.; Lin, C.: A mathematical model for split point drill flanks. *J. Eng. Ind.* **105**(3), 137–142 (1983). doi:[10.1115/1.3185879](https://doi.org/10.1115/1.3185879)
8. Tsai, W.D.; Wu, S.M.: A mathematical model for drill point design and grinding. *J. Eng. Ind.* **101**(3), 333–340 (1979). doi:[10.1115/1.3439515](https://doi.org/10.1115/1.3439515)
9. Tandon, P.; Gupta, P.; Dhande, S.G.: Modeling of twist drills in terms of 3D angles. *Int. J. Adv. Manuf. Technol.* **38**(5-6), 543–550 (2008). doi:[10.1007/s00170-007-1150-5](https://doi.org/10.1007/s00170-007-1150-5)
10. Paul, A.; Kapoor, S.G.; DeVor, R.E.: Chisel edge and cutting lip shape optimization for improved twist drill point design. *Int. J. Mach. Tools Manuf.* **45**(4-5), 421–431 (2005). doi:[10.1016/j.ijmactools.2004.09.010](https://doi.org/10.1016/j.ijmactools.2004.09.010)
11. Fujii, S.; DeVries, M.F.; Wu, S.M.: An analysis of drill geometry for optimum drill design by computer. Part II—computer-aided design. *J. Eng. Ind.* **92**(3), 657–666 (1970). doi:[10.1115/1.3427828](https://doi.org/10.1115/1.3427828)
12. Fujii, S.; DeVries, M.F.; Wu, S.M.: An analysis of drill geometry for optimum drill design by computer. Part I—drill geometry analysis. *J. Eng. Ind.* **92**(3), 647–656 (1970). doi:[10.1115/1.3427827](https://doi.org/10.1115/1.3427827)
13. Kang, S.K.; Ehmann, K.F.; Lin, C.: A CAD approach to helical groove machining—I. Mathematical model and model solution. *Int. J. Mach. Tools Manuf.* **36**(1), 141–153 (1996). doi:[10.1016/0890-6955\(95\)92631-8](https://doi.org/10.1016/0890-6955(95)92631-8)
14. Kang, S.K.; Ehmann, K.F.; Lin, C.: A CAD approach to helical groove machining. Part 2: numerical evaluation and sensitivity analysis. *Int. J. Mach. Tools Manuf.* **37**(1), 101–117 (1997). doi:[10.1016/0890-6955\(95\)00039-9](https://doi.org/10.1016/0890-6955(95)00039-9)
15. Sheth, D.S.; Malkin, S.: CAD/CAM for geometry and process analysis of helical groove machining. *CIRP Ann. Manuf. Technol.* **39**(1), 129–132 (1990). doi:[10.1016/S0007-8506\(07\)61018-X](https://doi.org/10.1016/S0007-8506(07)61018-X)
16. Kaldor, S.; Rafael, A.M.; Messinger, D.: On the CAD of profiles for cutters and helical flutes-geometrical aspects. *CIRP Ann. Manuf. Technol.* **37**(1), 53–56 (1988). doi:[10.1016/S0007-8506\(07\)61584-4](https://doi.org/10.1016/S0007-8506(07)61584-4)
17. Radhakrishnan, T.; Kawlra, R.K.; Wu, S.M.: A mathematical model of the grinding wheel profile required for a specific twist drill flute. *Int. J. Mach. Tool Des. Res.* **22**(4), 239–251 (1982)
18. Ehmann, K.F.; DeVries, M.F.: Grinding wheel profile definition for the manufacture of drill flutes. *CIRP Ann. Manuf. Technol.* **39**(1), 153–156 (1990). doi:[10.1016/S0007-8506\(07\)61024-5](https://doi.org/10.1016/S0007-8506(07)61024-5)
19. Chang, W.-T.; Chen, T.-H.; Tarn, Y.-S.: Measuring characteristic parameters of form grinding wheels used for microdrill fluting by computer vision. *Trans. Can. Soc. Mech. Eng.* **35**(3), 383–401 (2011)
20. Hinds, B.K.; Treanor, G.M.: Analysis of stresses in micro-drills using the finite element method. *Int. J. Mach. Tools Manuf.* **40**(10), 1443–1456 (2000). doi:[10.1016/S0890-6955\(00\)00007-9](https://doi.org/10.1016/S0890-6955(00)00007-9)
21. Chen, W.-C.: Applying the finite element method to drill design based on drill deformations. *Finite Elem. Anal. Des.* **26**(1), 57–81 (1997). doi:[10.1016/S0168-874X\(96\)00071-6](https://doi.org/10.1016/S0168-874X(96)00071-6)
22. Abele, E.; Fujara, M.; Schäfer, D.: Holistic approach for a simulation-based twist drill geometry optimization. In: *ASME 2011 International Manufacturing Science and Engineering Conference*, pp. 137–144 (2011). doi:[10.1115/MSEC2011-50102](https://doi.org/10.1115/MSEC2011-50102)
23. Selvam, S.V.M.; Sujatha, C.: Twist drill deformation and optimum drill geometry. *Comput. Struct.* **57**(5), 903–914 (1995). doi:[10.1016/0045-7949\(94\)00615-A](https://doi.org/10.1016/0045-7949(94)00615-A)
24. Yan, L.; Jiang, F.: A practical optimization design of helical geometry drill point and its grinding process. *Int. J. Adv. Manuf. Technol.* **64**(9-12), 1387–1394 (2013). doi:[10.1007/s00170-012-4109-0](https://doi.org/10.1007/s00170-012-4109-0)
25. Zhang, W.; Wang, X.; He, F.; Xiong, D.: A practical method of modelling and simulation for drill fluting. *Int. J. Mach. Tools Manuf.* **46**(6), 667–672 (2006). doi:[10.1016/j.ijmactools.2005.07.007](https://doi.org/10.1016/j.ijmactools.2005.07.007)
26. Shiou, F.J.; Hung, K.H.: Determination of the optimal geometrical features of a microdrill. *Appl. Mech. Mater.* **284**, 702–706 (2013)
27. Jain, K.C.; Chitale, A.K.: *Textbook of Production Engineering*. PHI Learning (2010)
28. Shaw, M.C.: *Metal Cutting Principles*. Clarendon Press, Oxford (1984)

